Available online at www.sciencedirect.com
SCIENCE DIRECT®
International Journal of Pharmaceutics 303 (2005) 72–80
international journal of pharmaceutics
www.elsevier.com/locate/ijpharm

Flow rate of some pharmaceutical diluents through die-orifices relevant to mini-tableting

K. Kachrimanis *, M. Petrides, S. Malamataris

Department of Pharmaceutical Technology, School of Pharmacy, University of Thessaloniki, Thessaloniki 54124, Greece

Received 4 April 2005; received in revised form 30 June 2005; accepted 1 July 2005
Available online 19 August 2005

Abstract

The effects of cylindrical orifice length and diameter on the flow rate of three commonly used pharmaceutical direct compression diluents (lactose, dibasic calcium phosphate dihydrate and pregelatinised starch) were investigated, besides the powder particle characteristics (particle size, aspect ratio, roundness and convexity) and the packing properties (true, bulk and tapped density). Flow rate was determined for three different sieve fractions through a series of miniature tableting dies of different orifice diameter (0.4, 0.3 and 0.2 cm) and thickness (1.5, 1.0 and 0.5 cm). It was found that flow rate decreased with the increase of the orifice length for the small diameter (0.2 cm) but for the large diameter (0.4 cm) was increased with the orifice length (die thickness). Flow rate changes with the orifice length are attributed to the flow regime (transitional arch formation) and possible alterations in the position of the free flowing zone caused by pressure gradients arising from the flow of self-entrained air, both above the entrance in the die orifice and across it. Modelling by the conventional Jones–Pilpel non-linear equation and by two machine learning algorithms (lazy learning, LL, and feed-forward back-propagation, FBP) was applied and predictive performance of the fitted models was compared. It was found that both FBP and LL algorithms have significantly higher predictive performance than the Jones–Pilpel non-linear equation, because they account both dimensions of the cylindrical die opening (diameter and length). The automatic relevance determination for FBP revealed that orifice length is the third most influential variable after the orifice diameter and particle size, followed by the bulk density, the difference between bulk and tapped densities and the particle convexity.

Keywords: Powder flow rate; Mini-tableting; Neural networks; Lazy learning

1. Introduction

Flowability is crucial for the success of mini-tableting and the required flow properties of the employed pharmaceutical powdered materials have been outlined (Flemming and Mielck, 1995). In general, flow properties are determined by a combination of (i) material properties (particle size, size distribution, shape, packing density and surface properties) and (ii) operating conditions (moisture, temperature, static charge and history of applied stresses). Stresses may arise from gravity and constrains imposed by the

* Corresponding author. Tel.: +30 2 310997666; fax: +30 2 310997652.
E-mail address: kgk@pharm.auth.gr (K. Kachrimanis).

0378-5173/$ – see front matter © 2005 Elsevier B.V. All rights reserved.
doi:10.1016/j.ijpharm.2005.07.003

containers during delivery into the die of tableting machine.

Until now the quantitative assessment of flow for pharmaceutical powdered materials in the context of tableting (with flow meters), as well as the prediction of critical flowability (with models and equations), is based on circular orifices. These orifices are considered as two-dimensional although recent studies have shown significant effects of die geometry and presence of air or vacuum in a shoe-die-filling system resembling tableting (Wu et al., 2003; Sinka et al., 2004). Furthermore, friction and flow of air during powder flow down a narrow vertical pipe (0.3 mm) were found to be dependent on the flow regime of the powder (Bertho et al., 2002). However, in mini-tableting where the orifice diameter is small, the "empty annulus" or the distance within which no particle centre can approach to the orifice edge, as well as the effects of air flow and pressure differences (gradients) caused by the powder movement (dilation) cannot be neglected. Especially the pressure gradients: (a) above the edge of the orifice due to difference between the velocities in the slow, fast and free-falling zones and (b) along the die-orifice (pipe), arising from the expansion of the self-entrained air (less than atmospheric—negative) (Crewdson et al., 1977; Bertho et al., 2002). All these may lead to the development of forces that alter the particle speed and can be related to serious implications in the filling of the die during mini-tableting. Furthermore, such effects should be taken into account for a rational correlation between flow rate measurements through orifices and weight variation of mini-tablets.

In the present study, we set out to explore and elucidate the effects of orifice dimensions (orifice length and diameter of the die) and of some powder particle characteristics (particle size, aspect ratio, roundness and convexity) and derived packing properties (true, bulk and tapped density) on the flow rate of some diluents employed in tableting by direct compression. Three sieve fractions of three common pharmaceutical diluents are employed. The experimental data are modelled with the help of Jones–Pilpel (JP) non-linear equation (Jones and Pilpel, 1966) as well as with different machine learning algorithms, and their predictive performance is assessed according to a two-way ANOVA design (Rasmussen et al., 1996). Finally, the input variable importance is evaluated.

2. Materials and methods

2.1. Materials

Direct compression lactose (DCL 21, DMV International, Veghel, The Netherlands), dibasic calcium phosphate dihydrate, DCPD (Emcompress®, Edward Mendell, NY, USA) and pregelatinised starch 1500 (Colorcon Ltd., Orpington, UK) were used after classification by passing through a nest of sieves (90, 125, 150, 180 and 250 μm, Endecotts, England) employing a vibrating sieve shaker (ILM Veb Labor, Type THYR, Germany) at high intensity level (No. 5/6) for 10 min. For starch 1500 fraction larger than 250 μm was not obtained, while for lactose the <90 μm fraction did not flow through the orifices used in this study and the fractions 90–125 and 125–150 μm had to be mixed in order to obtain sufficient quantity for experimentation. Therefore, three representative size fractions were selected (Table 1), which were different for each diluent and are designated as Large (L), Medium (M) and Small (S).

2.2. Particle characteristics and packing properties of powders

Particle characteristics (size, aspect ratio, roundness and convexity) and packing properties (true, bulk and tapped density) of the powders were measured by previously described in detail methods (Kachrimanis et al., 2003).

2.3. Flow measurement

Flow rate through a series of miniature tableting dies differing in orifice diameter (0.4, 0.3 and 0.2 cm) and thickness (1.5, 1.0 and 0.5 cm) was measured by employing a specially constructed flow meter, which was earthed, in order to avoid electrostatic charging. It consisted of an electronic balance with a precision of ±0.1 g (A&D Ltd., Japan) connected to a PC through an RS232 serial communication for monitoring of powder flow, and a glass cylindrical hopper, as described in detail elsewhere (Kachrimanis et al., 2003). Powder was transferred in the hopper up to a certain height (5 cm), to imitate the conditions of a tableting machine. Data were logged every 0.2 s with the help of Windmill serial communication software (Windmill, UK)

Table 1
Particle characteristics and packing properties of the fractionated diluents

Diluent	Sieve fraction (size, μm)	Density (kg/m^3)			Particle diameter CED (μm)	Aspect ratio	Roundness	Convexity
		True (ρ_t)	Bulk (ρ_b)	Tap − bulk ($\rho_t - \rho_b$)				
Lactose (DCL 21)	L (>250)	1540	638	76	367.5	1.34	1.22	1.07
	M (180–150)	1540	631	88	262.6	1.41	1.26	1.07
	S (150–90)	1540	633	92	146.3	1.43	1.28	1.08
DCPD (Emcompress®)	L (>250)	2390	813	127	240.6	1.33	1.41	1.13
	M (180–150)	2390	791	129	202.7	1.54	1.73	1.16
	S (125–90)	2390	801	119	136.6	1.40	1.47	1.14
Starch (STARCH 1500)	L (180–150)	1500	678	60	184.6	1.61	1.50	1.12
	M (125–90)	1500	658	88	151.1	1.34	1.23	1.08
	S (<90)	1500	650	97	117.4	1.34	1.27	1.08

and transferred to MS Excel. Powder flow rate (g/s) was estimated from the slope of flowing mass versus time plots (Fig. 1) by linear regression including all data, and expressed as mean linear velocity of the falling particles (cm/s), at the orifice inlet, calculated by dividing the cross sectional area normalised flow rate with the bulk density of the powder. All experiments were conducted in a room of controlled relative humidity (50%) employing a dehumidifier (Pretema AG, Zurich, Swiss) and flow rate determinations were repeated in triplicate.

In order to elucidate the mechanism of powder flow, a sequence of microphotographs of the flowing powder was taken at different vertical distance from the die outlet, using a Nikon Coolpix 4500 digital camera (4.0 MPixel resolution, frame rate 35 s^{-1}) mounted on a horizontally located Olympus SZX stereoscope.

2.4. Data modelling

2.4.1. Data sets

The experimental data of flow rate comprised a full factorial design, replicated three times. The factors were: diluent (represented by its true density, at three levels), sieve fraction (as measured circle equivalent diameter, CED, at three levels), orifice diameter and thickness of the die (each at three levels).

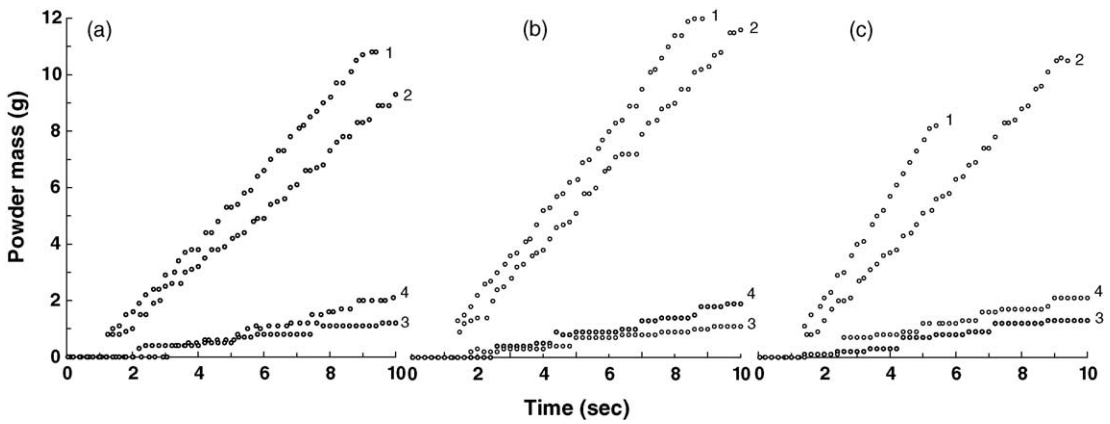

Fig. 1. (a–c) Typical flowing mass vs. time plots for the small sieve fraction of the diluents: lactose (a), DCPD (b) and starch (c). Orifice diameter/length: 0.4 cm/1.5 cm (1), 0.4 cm/0.5 cm (2), 0.2 cm/1.5 cm (3) and 0.2 cm/0.5 cm (4).

Nine variables were selected as inputs to the FBP and LL algorithms: (1) bulk density, ρ_b, (2) difference between bulk and tapped densities, $\rho_t - \rho_b$, (3) orifice diameter, D_o, (4) particle size, CED, (5) aspect ratio, (6) roundness, (7) convexity, (8) true density and (9) orifice length or thickness of the die. The corresponding true density represented the diluent, so that no categorical variable was included as input, and the measured particle mean diameter (CED) was used instead of the nominal sieve size fraction, as a more realistic estimate of particle size. The values of CED were different from the nominal sieve size especially in the case of lactose (Table 1) and this can be attributed to the greater deviation from sphericity due to the elongated habit of lactose crystals. The input and output patterns were scaled in the interval]0, 1[with 10% headroom, where the sigmoid function operates in the more linear region (Murtoniemi et al., 1994). The data were split into three disjoint training sets with increasing number of data points (60, 100 and 140), and three corresponding test sets of 25 points.

2.4.2. Models and fitting

The (JP) equation, Eq. (1), and two machine learning algorithms representative of different computing approaches were fitted to the data: the lazy learning (LL) algorithm and a standard feed-forward back-propagation (FBP) neural network.

The JP equation is applicable to single component as well as multi-component mixtures:

$$D_o = A\left(\frac{4W}{60\pi(\rho_b)\sqrt{g}}\right)^{1/n} \quad (1)$$

where A and n are coefficients determined experimentally, that quantify the effects of many variables (material or operator). It is a more general form of the equation proposed by Beverloo et al. (1961):

$$W = C\rho_b g^{1/2}(D_o - Z)^{5/2} \quad (2)$$

where W is the flow rate, D_o the orifice diameter, ρ_b the material bulk density, g the gravitational acceleration, while C and Z are two empirical parameters determined experimentally. Constant C depends on the value of ρ_b and acquires values in the range 0.55–0.65. Z is correlated with particle size, d, according to the relation:

$$Z = kd \quad (3)$$

where k is a function of particle shape with values smaller than one ($k < 1$) that can give the "empty annulus" or the distance ($kd/2$) within which no particle center can approach to the orifice edge (Brown and Richards, 1965).

The lazy learning is a local modelling technique focusing attention to the sub-region neighbouring of the point that is being estimated, instead of utilizing the whole data set. The algorithm postpones all computations until a prediction is requested and then it proceeds in interpolation of the relevant examples according to some measure of distance. The back-propagation neural network consisted of a single hidden layer of 10 units, a single output unit and no shortcut connections (Fig. 2). It was trained by the scaled conjugate gradient algorithm, with Bayesian regularisation of the weights, for 300 cycles. The linear activation function was selected for the input and output units and the logistic sigmoid function for the hidden units. Different initial weights were used with each training-set, so that the effect of the stochastic component (random initialisation) on the error of prediction was confounded with the effect of training set distribution.

The JP model was fitted to the measured mass flow rate data (g/s) by non-linear regression using the JMP-IN ver. 5.1 (SAS Institute Inc.). For the application of the machine learning algorithms, the MATLAB software was used (Mathworks Inc.), and specifically, the Lazy Learning package (Birattari et al., 1999) and the Netlab Toolbox (Nabney, 2001).

2.4.3. Statistical analysis of results

The performance of the models was assessed by evaluating the mean and variance of the generalisation error expressed as the squared difference of observed minus predicted values. Sources of variation in the generalisation error may be: (a) the random components of the learning algorithms, (b) the size and distribution of the training sets and (c) the distribution of test data. A hierarchical model was applied to isolate the sources of variation (Rasmussen et al., 1996). The expectation of generalisation (prediction) error was given by:

$$y_{ij} = \mu + \alpha_i + \varepsilon_{ij} \quad (4)$$

where y_{ij} is the loss on training set i and test case j, μ the overall mean generalisation error, α_i a random variable that explains the effect on μ_n due to the choice of

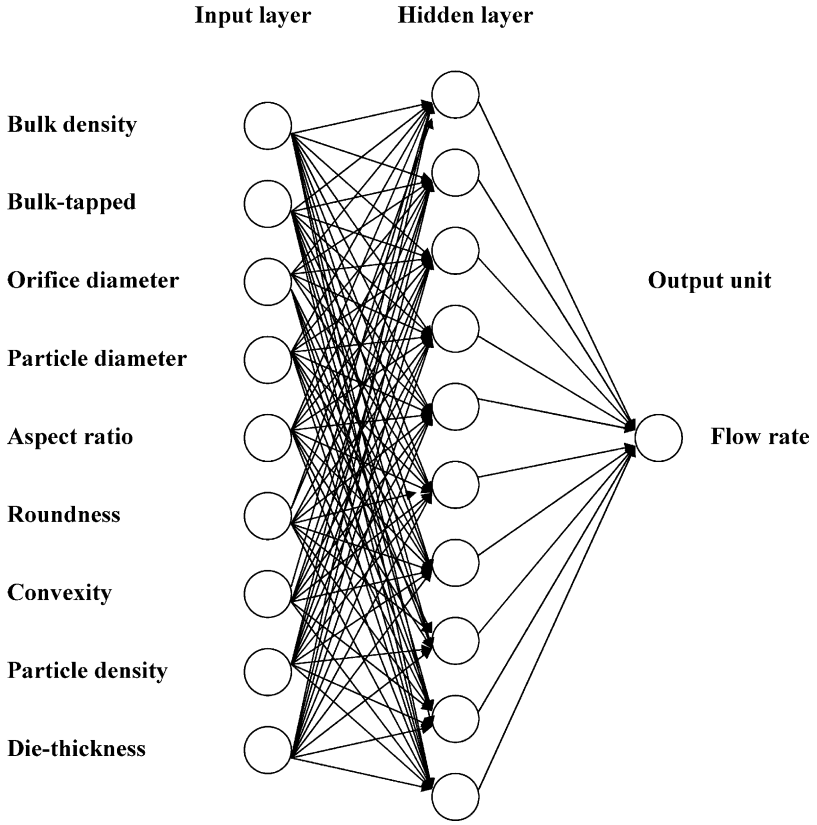

Fig. 2. Topology of the feed-forward back-propagation (FBP) neural network. Nine units in the input layer, 10 units in a single hidden layer and a single output unit with no shortcut connections.

training set and ε_{ij} is the error term, which accounts for all errors unexplained by the model. The mean overall performance and its standard deviation for each algorithm were estimated. Eq. (4) was used to model the difference between the losses of the two algorithms, k and k'.

$$y_{ijk} - y_{ijk'} = \Delta\mu + \Delta\alpha_i + \Delta\varepsilon_{ij} \quad (5)$$

Finally, the hypothesis that the estimated overall difference does not deviate significantly from zero was tested, by performing a paired t-test.

2.5. Importance of input variables

Importance of the input variables was determined for the FBP model by the "automatic relevance determination", ARD routine, implemented in the Netlab package (Neal, 1996). The hyper-parameters of the prior distribution of the weights associated with each input variable were calculated in terms of the Bayesian theory of probability. Variables with lower hyper-parameter values are considered as the most important because they correspond to inverse variance estimates.

3. Results and discussion

3.1. Effects on flow

In Fig. 1(a–c) are shown typical plots of flowing powder mass versus time for the small sieve fraction of the diluents, and in Fig. 3(a–c) plots of mean linear velocity of the falling particles, at the orifice inlet, versus ratio of orifice diameter/length of the die.

Figs. 1 and 3 show that flow rate, for given fraction and orifice dimensions, increases in the order:

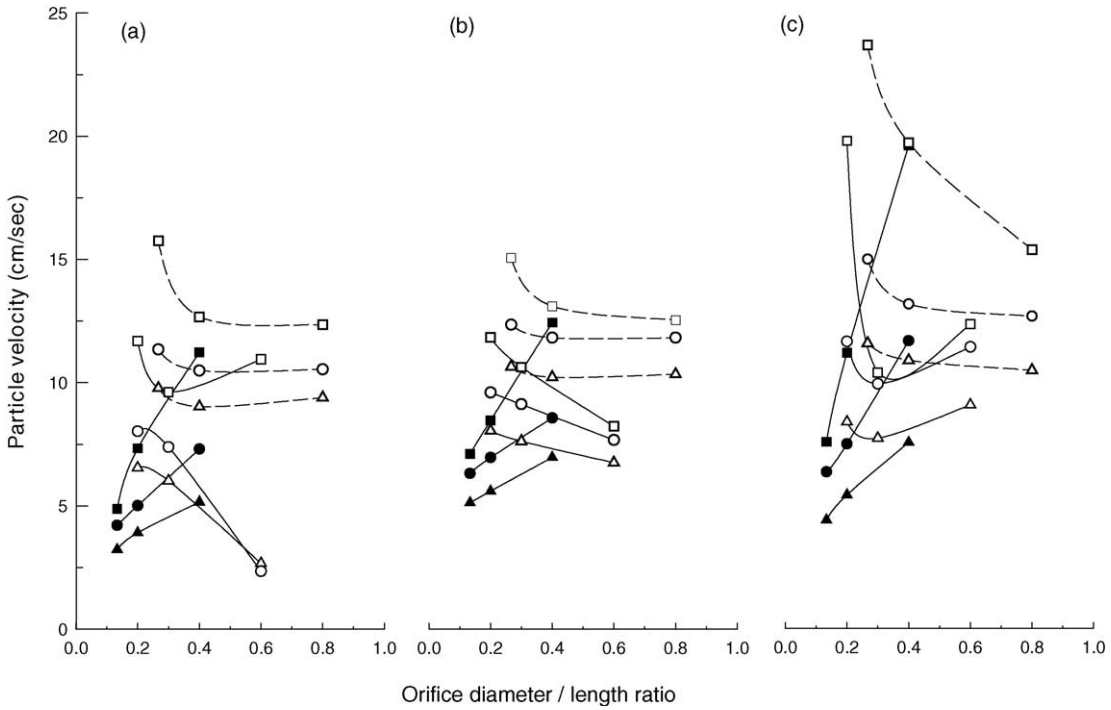

Fig. 3. (a–c) Mean linear velocity of falling particles vs. the orifice diameter/length ratio for the diluent: lactose (a), DCPD (b) and starch (c). Orifice diameter: 0.2 cm (full symbols and continuous lines), 0.3 cm (empty symbols and continuous lines) and 0.4 cm (empty symbols and dashed lines). Particle size fraction: Large (triangles), Medium (circles) and Small (squares).

lactose < DCPD < starch. These differences should be attributed to the alterations in the interparticle mechanical (frictional) and physical (attractive) forces due to differences in particle shape and surface roughness as well as due to the gravitational forces resulting from the different particle densities.

Furthermore, Fig. 3(a–c) shows a reduction of mean linear particle velocity as the particle size increases, for the particle size range and orifice dimensions studied, although the interparticle attractive force decreases while the gravitational force exerted on the particles increases. This is an indication that a process of unstable (transitional) arch formation and collapse dominates powder flow. This process is also evidenced by the "stepped" patterns of the mass flow versus time plots, in Fig. 1, and particularly for plots 1 and 2, which show that powder flow rate periodically accelerates, probably as the transitionally formed above the orifice arch is destroyed. Furthermore, this process is confirmed by the sequential photographic monitoring of flow presented in Fig. 4, showing the instability in the flow regime.

Additionally, Fig. 3 shows that there is a general decrease in the flow rate as the length of the orifice increases for the small orifice diameter (0.2 cm), a partial decrease for the intermediate diameter (0.3 cm) and an increase for the large diameter (0.4 cm). This dependence of flow rate change with orifice length on the diameter size means significant three-dimensional effects for the occurring flow regime, intermediate between stationary free-fall and steady-wave regime (Wu et al., 2003; Srivastava and Sundaresan, 2003). Therefore, the pressure gradients above and bellow the free falling zone may alter the conditions controlling the formation and collapse of the transitional arch or the position of the free falling zone relatively to the upper edge of the die-orifice (Crewdson et al., 1977; Bertho et al., 2002).

For the small diameter (0.2 cm), the reduction of particle velocity due to increase of orifice length (cor-

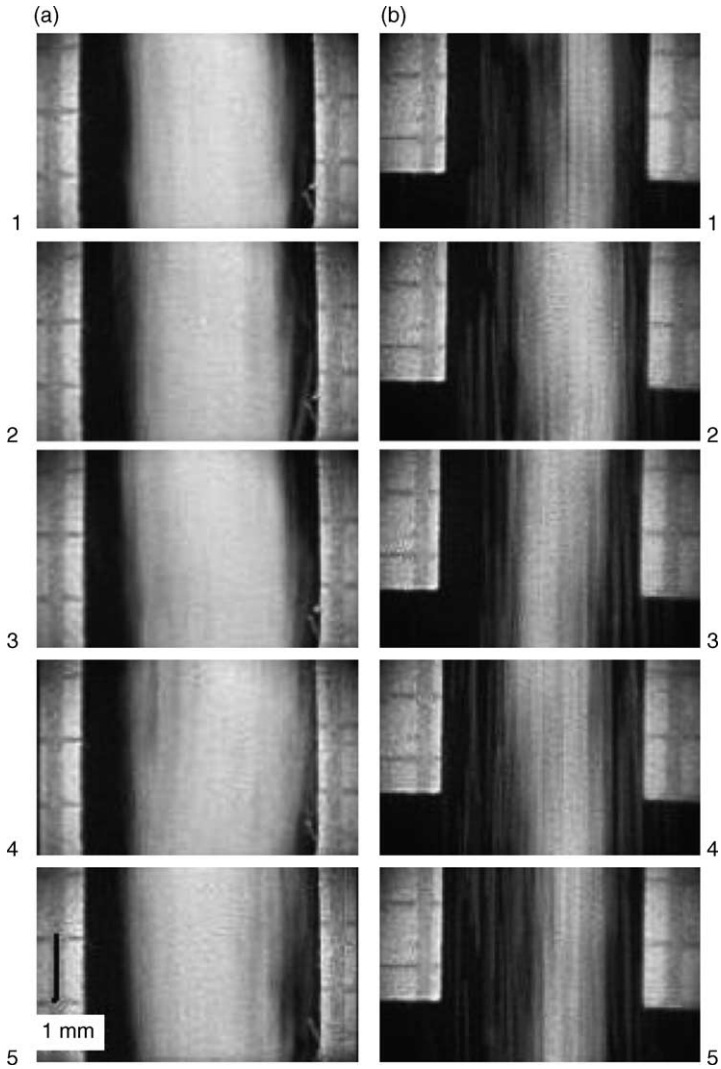

Fig. 4. Photographs of the flowing powder at the orifice outlet (a) and 2 cm bellow (b), taken at 0.028 s intervals.

responding to decreased diameter/length ratio) reflects the limitations in particle mobility and separation and predominance of interparticle frictional and attractive forces. Therefore, increase of negative pressure gradient across the orifice with the die-thickness (Bertho et al., 2002), presumably results in reduction of powder dilation across the die-orifice and increased wall friction. This should cause increase of interparticle frictional and attractive forces both below and above the free falling zone and in decrease of particle velocity. On the contrary, for the large orifice (0.4 cm) the negative pressure gradient along the die-orifice should not be significant probably because the flow regime in this case should be more likely as stationary free-fall than steady-wave. Therefore, predominance of pressure gradient above the free falling zone may be combined with lowering of free-falling zone and transitional arch towards the entrance of the cylindrical hole and probably downwards to the orifice outlet. The possibility of this lowering of the level at which transition of solid flow from granular to suspended occurs, increases with the orifice length and this should result in

Table 2
Overall and marginal predictive performance

Model	Overall M.S.E.$_p$ (kg s^{-1}, $\times 10^6$)	Marginal M.S.E.$_p$ (kg s^{-1}, $\times 10^6$) for training set size		
		60 points	100 points	140 points
JP	10.70 ± 2.27	8.64 ± 12.21	9.75 ± 15.73	13.72 ± 20.10
LL	3.99 ± 2.20	8.40 ± 25.86	1.59 ± 3.79	1.99 ± 5.57
FBP	3.49 ± 2.45	8.37 ± 25.75	0.62 ± 1.09	1.49 ± 3.85

Mean squared error of prediction (M.S.E.$_p$), standard error (S.E.) and standard deviation (S.D.). The values are overall mean ± S.E. and marginal mean ± S.D.

increased rearrangement and dilation above the particle free falling with the die-thickness increase. In other words, the upper edge of the die-orifice should act as a baffle increasing the powder dilation and not as particle brake, like the case of small orifice. This may result in increased powder dilation and particle velocity caused by increased predominance of gravitational over frictional and attractive forces, as the die-thickness increases.

3.2. Flow modelling

In Table 2 are listed the overall mean and the marginal predictive performance of the training sets. In Table 3 are listed the probability levels for the statistical significance of the pair-wise differences in the overall mean and marginal (referring to each subset of the data separately) predictive performance of the models, calculated by the paired *t*-test.

From the values of Table 2 it is seen that both machine learning algorithms (LL and FBP) achieve smaller overall M.S.E.$_p$ than the JP model. However, looking at the marginal M.S.E.$_p$ we can see that it is dependent upon the data distribution. For the JP model, the predictive performance seems to deteriorate, as more data are available for training, while the FBP and LL algorithms improve their predictive performance as the data sets become larger. This can be clearly seen in the data of Table 3, where the overall M.S.E.$_p$ of the FBP and LL algorithms is significantly smaller than that of the JP model (*p*-level 0.003 and 0.001, for the JP-LL and JP-FBP comparison, respectively), while the marginal M.S.E.$_p$ for the smallest data set shows no statistically significant differences between the models. Finally, no significant difference either in the overall or in the marginal M.S.E.$_p$ was found between the LL and the FBP neural network.

Bad predictive performance is expected with a small data set since it might not contain enough information. However, the deterioration of predictive performance for the JP model even when more data are available, suggests its strong dependence on data distribution. Therefore, FBP and LL algorithms are advantageous in modelling flow rate, since they are more robust in changes of the training data distribution.

3.3. Importance of input variables

In Table 4 are listed the hyper-parameters expressing the importance of the variables under investigation which were obtained by the automatic relevance determination (ARD) method as a function of training set

Table 3
Probability levels for the statistical significance of the pair-wise differences in the overall and marginal predictive performance (M.S.E.$_p$) calculated by the paired *t*-test of the models

Model	Overall M.S.E.$_p$		Marginal M.S.E.$_p$ for data points					
	LL	FBP	60		100		140	
			LL	FBP	LL	FBP	LL	FBP
JP	0.003	0.001	0.481	0.477	0.010	0.004	0.004	0.003
LL	–	0.454	–	0.209	–	0.670	–	0.498
FBP	0.546	–	0.791	–	0.330	–	0.502	–

Table 4
Hyper-parameters for the importance of input variables estimated by the automatic relevance determination (ARD) method as a function of training set size

Variable	60 points	100 points	140 points
X_1: bulk density (ρ_b)	94.3 (5)	76.0 (7)	19.4 (5)
X_2: tapped − bulk ($\rho_t - \rho_b$)	156.8 (6)	19.9 (4)	6.7 (4)
X_3: orifice diameter	2.0 (1)	2.7 (1)	1.9 (1)
X_4: particle diameter	4.1 (2)	6.6 (2)	2.5 (2)
X_5: aspect ratio	318.8 (8)	81.2 (8)	171.3 (9)
X_6: roundness	254.7 (7)	53.9 (5)	75.8 (7)
X_7: convexity	31.6 (4)	106.4 (9)	34.9 (6)
X_8: true density (ρ_t)	492.5 (9)	54.4 (6)	107.2 (8)
X_9: orifice length	16.9 (3)	9.8 (3)	6.5 (3)

Numbers in parentheses indicate the rank order of variable importance.

size. They show that, in general, the variables with lower ARD values (more important) are the orifice diameter, the particle size and the length of the cylindrical orifice. Also, they show that importance of the bulk density (ρ_b), the difference of bulk and tapped densities ($\rho_t - \rho_b$), and the particle convexity greatly depends on the training set size or data distribution. The first two variables (ρ_b and $\rho_t - \rho_b$) are not important when the FBP model is "trained" (fitted) on the small (60 points) and medium (100 points) data sets but their importance increases for the larger (140 points) data set. Particle convexity has moderate importance for the smallest and largest data sets but it is not important for the medium data set. From all the aforementioned, it becomes clear that both dimensions of the die-opening (orifice diameter and length) affect significantly the flow rate, and this is the reason for the better performance of the FBP and LL algorithms compared to the JP equation, which was not developed to account for any effect of the third dimension of the hole. Possible implication of this finding may be improvement of mini-tablet weight uniformity by applying optimisation based on orifice diameter, particle size and die-depth.

4. Conclusions

The flow rate generally decreases as the thickness of the mini-tableting die increases for the smaller orifice diameter (0.2 cm), while there is an increase with orifice length (die-thickness) for the largest orifice diameter (0.4 cm). Both machine learning algorithms (LL and FBP) account the effects of the die-thickness and diameter and have better predictive performance than the conventional non-linear (JP) model. Most influential variables, in descending order of significance, determined for the FBP model, were the orifice diameter, the particle size, and the orifice length (die-thickness), followed by the bulk density, the difference between bulk and tapped densities and the particle convexity.

References

Bertho, Y., Girgiutti-Dauphine, F., Raafat, T., Hinch, E.J., Herrmann, H.J., Hulin, J.P., 2002. Powder flow down a vertical pipe: the effect of air flow. J. Fluid Mech. 459, 317–345.

Beverloo, W., Leniger, H., Van de Velde, J., 1961. The flow of granular solids through orifices. Chem. Eng. Sci. 15, 260–269.

Birattari, M., Bontempi, G., Bersini, H., 1999. Lazy learning meets the recursive least-squares algorithm. In: Kearns, M.S., Solla, S.A., Cohn, DA. (Eds.), Advances in Neural Information Processing Systems, vol. 11. MIT Press, Cambridge, MA, pp. 375–381.

Brown, R.L., Richards, J.C., 1965. Kinematics of the flow of dry powders and bulk solids. Rheol. Acta 4, 153–165.

Crewdson, B.J., Ormond, A.L., Nedderman, R.M., 1977. Air-impeded discharge of fine particles from a hopper. Powder Technol. 16, 197–207.

Flemming, J., Mielck, J.B., 1995. Requirements for the production of micro-tablets: suitability of direct-compression excipients estimated from powder characteristics and flow rates. Drug Dev. Ind. Pharm. 21, 2239–2251.

Jones, T., Pilpel, N., 1966. The flow properties of granular magnesia. J. Pharm. Pharmacol. 18, 81–93.

Kachrimanis, K., Karamyan, V., Malamataris, S., 2003. Artificial neural networks (ANNs) and modeling of powder flow. Int. J. Pharm. 250, 13–23.

Murtoniemi, E., Yliruusi, J., Kinnunen, P., Merkku, P., Leiviskä, K., 1994. The advantages by the use of neural networks in modelling the fluidised bed granulation process. Int. J. Pharm. 108, 155–164.

Nabney, I., 2001. NETLAB Algorithms for Pattern Recognition. Advances in Pattern Recognition Series. Springer-Verlag, Heidelber.

Neal, R.M., 1996. Bayesian Learning for Neural Networks. Lecture Notes in Statistics. Springer, New York.

Rasmussen, C., Neal, R., Hinton, G., van Camp, D., Revow, M., Ghahramani, Z., Kustra, R., Tibshirani, R., 1996. The DELVE Manual, 1.1 ed. Department of Computer Science, University of Toronto, Canada, http://www.cs.utoronto.ca/∼delve/.

Sinka, I.C., Schneider, L.C.R., Cocks, A.C.F., 2004. Measurement of the flow properties of powders with special reference to die fill. Int. J. Pharm. 280, 27–38.

Srivastava, A., Sundaresan, S., 2003. Analysis of a frictional-kinetic model for gas-particle flow. Powder Technol. 129, 72–85.

Wu, C.Y., Dihoru, L., Cocks, A.C.F., 2003. The flow of powder into simple and stepped dies. Powder Technol. 134, 24–39.